

Quasi-BIC laser enabled by high-contrast grating resonator for gas detection

Haoran Zhang^{1,2}, Tao Wang^{1,2}, Jiacheng Sun^{1,3}, Shaoxian Li^{1,2}, Israel De Leon⁴, Remo Proietti Zaccaria⁵, Liang Peng^{1,2}, Fei Gao⁶, Xiao Lin⁶, Hongsheng Chen⁶, GaoFeng Wang^{1,2}

¹*Engineering Research Center of Smart Microsensors and Microsystems of MOE, Hangzhou Dianzi University, Hangzhou, 310018, China*

²*School of Electronics and Information, Hangzhou Dianzi University, Hangzhou, 310018, China*

³*School of Zhuoyue Honors, Hangzhou Dianzi University, Hangzhou, 310018, China*

⁴*School of Engineering and Sciences, Tecnológico de Monterrey, Monterrey, Nuevo León 64849, Mexico*

⁵*Cixi Institute of Biomedical Engineering, Ningbo Institute of Materials Technology and Engineering, Chinese Academy of Sciences; Italian Institute of Technology via Morego 30, 16163 Genova, Italy and*

⁶*Interdisciplinary Center for Quantum Information, College of Information Science and Electronic Engineering, Zhejiang University, Hangzhou 310027, China*
(Dated: July 21, 2022)

In this work, we propose and numerically investigate a new kind of two-dimensional microcavity resonator, consisting of an organic Rhodamine 6G doped SiO₂ thin layer sandwiched between two symmetric high-contrast-grating (HCG) layers. The larger periodic-index-contrast from the grating enables an ultra-high (99%) reflectivity over a broad spectrum. Meanwhile, the so-called bound states in continuum (BIC) are supported upon a proper choice of topological parameters. Since the high-index dielectric configuration favors strong electric and magnetic resonances, then a quasi-BIC laser with ultra low threshold (pump fluence of 17 $\mu\text{J}/\text{cm}^2$) and very narrow optical spectrum linewidth is successfully realized in the visible range. This innovative device displays distinguished sensing performance for gas detection, and the emission wavelength sensitively shifts to the longer wavelength with the changing of environment refractive index (in order of 5×10^{-4}). The achieved bulk sensitivity is 221 nm/RIU with a high signal to noise ratio, and a record-high figure of merit (FOM) reaches to 4420 RIU⁻¹. This ultracompact and low threshold quasi-BIC laser facilitated by the ultra-narrow resonance can serve as formidable candidate for on-chip gas sensor.

PACS numbers:

I. INTRODUCTION

In recent years, the investigation of bound states in the continuum (BICs) has attracted substantial attention due to the interesting physics and practical applications [1]. The BIC theory originated from quantum mechanics and was firstly proposed by von Neumann and Wigner in 1929 [2, 3]. Since then, it has been used to explain the important physical concept of destructive interference in various physical systems, such as photonics [4–7], acoustics [8, 9] and water waves [10]. According to Neumann and Wigner’s seminal work [2], when two resonances pass each other as a function of a continuous parameter, the two channels will interfere, and give rise to an avoided crossing for their resonances. Theoretically, at a given value of the continuous parameter, one of the channels vanishes entirely and hence becomes a dark mode (BIC mode) with an infinite quality (Q) factor [12]. In practice, BICs are limited by finite structure size, material absorption, and structural imperfection [20], they manifest themselves and collapse to Fano resonant states with long lifetime, also known as quasi-BICs [11, 21]. Recently, high- Q quasi-BICs have been observed in many passive systems, and it has been recognized that practical systems supporting such resonances are well suited for lasing and sensing applications [22, 23].

Sub-wavelength high-contrast gratings (HCGs) possess distinct features, such as broadband high reflectivity

(> 99%) and high- Q resonances (> 10^7) [46]. In particular, it has been shown that HCG systems can support symmetry-protected BICs with improved spectral performance [1, 24]. The narrow spectral linewidth (γ) featured by these structures are quite sensitive to changes in refractive index around them [25], making them promising candidates for engineering optical sensors with high sensitivity (S) and excellent figure of merit, $\text{FOM} = S/\gamma$ [26]. However, such kind of sensors are passive devices, and significantly less sensitivity [27]. Recent studies indicate that active sensors based on small lasers not only supply coherent radiation, but also show enhanced sensing performance [28, 29]. Thus, photonic structures supporting high- Q quasi-BIC lasers are of great interest in sensing applications, as they could offer possibilities of achieving a sensing performance beyond that of more conventional photonic sensors [30, 31].

Lasing action based on BICs or quasi-BICs in two-dimensional photonic-crystal structures has been reported recently [22, 23, 32]. Nonetheless, the relevant studies based on one-dimensional photonic-crystal structures are very rare. In this work, we propose an innovative resonator composed of highly reflecting HCG layers surrounding a thin organic-dye-doped SiO₂ layer working as gain material for laser emission. This ultracompact resonator design not only opens an alternative route to generate symmetry-protected resonance modes, but also provides a

platform to demonstrate a quasi-BIC laser by combining organic dye molecules with inorganic grating. Finite difference-time-domain (FDTD) numerical simulations have been performed to evaluate the performance of the aforementioned system with the results suggesting that a high- Q quasi-BIC mode ($Q > 10^4$) can be established by carefully optimizing the HCG structural parameters. Then, when the quasi-BIC mode spectrum overlaps with that of the gain material, a pronounced lasing action is obtained. More significantly, this quasi-BIC laser allows for a highly precise environment change detection through the reading of the emission wavelength shift. The achieved narrow linewidth (0.05 nm) combined with a large bulk sensitivity of 221 nm/RIU, results in a FOM of 4420 RIU⁻¹, which is approximately 20 times larger than typical passive sensors [33]. Therefore, our results indicate that the proposed quasi-BIC laser offers great potential for optical sensing of gases in low-concentration.

II. RESONATOR DESIGN AND NUMERICAL MODEL

A. Structure design

The schematic diagram of proposed HCG resonant structure is shown in Fig. 1. The structure is designed to support a resonance at a wavelength of 570 nm. The active region consists of 215 nm thick SiO₂ layer doped with Rhodamine 6G (R6G), as shown in Fig. 1(a). A similar gain medium has been reported in a previous work [34]. The R6G layer is surrounded by Si₃N₄ stripes with a symmetric arrangement along z direction, and the refractive index of Si₃N₄ is 2.0. The HCG parameters are described by the thickness of grating layer is T , filling factor (the grating width divided by the period) F and the period Λ . We consider the dimensions of whole device in x - and y -direction are infinite, as exhibited in Fig. 1(b). The detail parameters of materials are shown in Table 1.

A freestanding cascade grating fabrication technique, based on positive resist e-beam lithography (EBL) and ion coupling plasma, may be feasible to fabricate the designed structure. The SiO₂ layer doped with R6G can be made by using sol-gel technique, which is a suitable method for incorporating organic molecules into inorganic solid hosts. The low-temperature process involving the hydrolysis and condensation reactions of metal alkoxides enables us to dope different molecules with a poor thermal stability into coating films [35]. The fabrication process mainly includes thin film deposition and grating pattern. The Si₃N₄ thin film is uniformly coated with SiO₂ doped R6G sol solution, then cover another Si₃N₄ thin film on the other side. The grating structures can be separately patterned on both side by using EBL and ICP with CHF₃ gas [36]. A similar sandwiching structure consisting of two Al gratings and a Si₃N₄ membrane has been reported recently [37].

B. Theory and simulation

A semi-quantum framework is adopted to simulate the interaction between the electromagnetic fields and gain medium. The organic dye molecules in this work are well described as a four-energy-level system, and the population inversion is generated between the electronic level of L_2 state and L_1 state. As shown in Fig. 2, which presents the population dynamics of the four relevant electronic levels of the molecule, such as the ground state, L_0 , and the three excited states, L_1 , L_2 , and L_3 . The molecular polarization given by spontaneous and stimulated transitions are described through the following equation [38]:

$$\frac{d^2 \vec{P}_{i,j}}{dt^2} + \Delta\omega_{i,j} \frac{d\vec{P}_{i,j}}{dt} + \omega_{i,j}^2 \vec{P}_{i,j} = \kappa_{(i,j)} \Delta N_{i,j}(t) \vec{E}(t) \quad (1)$$

where $\Delta\omega_{i,j}$ and $\omega_{i,j}$ are the bandwidth and frequency of the transition between states i and j , $\kappa_{i,j} = 6\pi\epsilon_0 c^3 / (\omega_{i,j}^2 \cdot \tau_{i,j})$ [39], $\tau_{i,j}$ represents the lifetime of the spontaneous emission. $\Delta N_{i,j}(t)$ is the difference of population density between two energy states of the interest. $\vec{E}(t)$ is the total electric field, and can be calculated by solving the curl Maxwell equations [40]:

$$\nabla \times \vec{E}(t) = -\mu_0 \frac{\partial \vec{H}(t)}{\partial t}, \quad (2)$$

$$\nabla \times \vec{H}(t) = \epsilon \frac{\partial \vec{E}(t)}{\partial t} + \frac{\partial (\vec{P}_{30}(t) + \vec{P}_{21}(t))}{\partial t} \quad (3)$$

In order to solve for the fields in a self-consistent fashion, it is necessary to couple the molecular polarization $\vec{P}_{i,j}$ to the electromagnetic fields via the rate equations of the four-level system describing the gain medium [41]. Such rate equations describe the time evolution of the energy states' population densities, and are given by Ref. [42]. The time evolution of each energy state density is described by their respective spontaneous decay processes $N_i/(\tau_{i,j})$ and stimulated processes ($\vec{E}(t) \cdot d\vec{P}_{i,j}/dt$). The field involved in the rate equations is the total field and accounts for the effects of any local optical intensity on the dynamics of the population densities.

The FDTD technique is adopted to solve the coupled equations. For the case of R6G-doped SiO₂, we set that the absorption transition: $\lambda_a = 512$ nm and $\Delta\lambda_a = 35$ nm; the emission transition: $\lambda_e = 570$ nm and $\Delta\lambda_e = 50$ nm; the concentration of dye molecule: $C = 1 \times 10^{19}$ cm⁻³, which is comparable to the concentrations previously reported in the same material host [34]; and the lifetimes: $\tau_{32} = \tau_{10} = 5 \times 10^{-14}$ s, $\tau_{30} = 1 \times 10^{-9}$ s, $\tau_{21} = 1.8 \times 10^{-9}$ s. Finally, the calculated emission cross section is around 3×10^{-16} cm², which is also consistent with the experimental report [43].

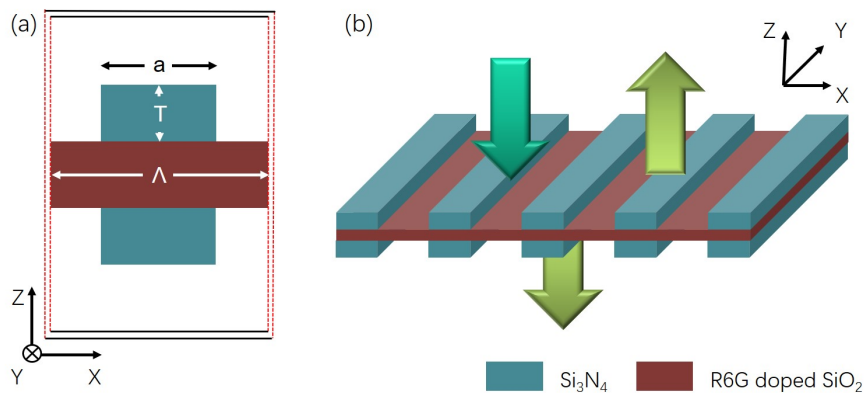


FIG. 1: The schematic of proposed resonator based on HCGs: (a) single unit cell of two dimensional resonator; (b) whole structure with the organic R6G thin layer. The green downward arrow represents optical pump, the reseda arrows on both sides of resonator are emitted light from the resonator.

Table 1. Material parameters

Layer	Material	Refractive index	Thickness (nm)
Top HCG	Si3N4	2.0	230
Gain	R6G-doped SiO2	1.46	215
Bottom HCG	Si3N4	2.0	230

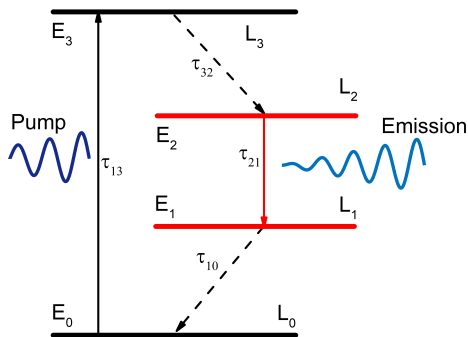


FIG. 2: Energy level diagram and parameters used for modelling the dye molecules in FDTD simulations. The transition energies are $E_{30} = E_3 - E_0$ and $E_{21} = E_2 - E_1$. Since the transition from L_3 to L_2 is much faster than the transition from L_3 to L_0 , the excitation quickly decay to L_2 , leading to a population inversion for the transition from L_2 to L_1 .

III. BOUND STATES IN THE CONTINUUM AND QUASI-BIC LASING

A. BIC modes supported by the passive structure

First, the optical properties of single HCG layer are analyzed. For this, we carry out FDTD simulations

and calculate the structure's reflectance, for a normally incident plane wave polarized along the y-direction. Fig. 3(a) illustrates the results of our simulations as a function of the wavelength and of the grating thickness, taking a grating filling fraction $F = 0.5$. We observe two regions, which we refer to as the dual/multi-mode region (from $\lambda = 530$ nm to 700 nm) and the single-mode region ($\lambda > 700$ nm), as suggested by previous nomenclature [45]. For the single mode region, the grating operates in a longer wavelength regime, behaving like a quasi-uniform layer [46], so only Fabry-Perot modes are supported in this wavelength range. On the other hand, in the dual/multi-modes region, the pattern is quite different, describing contrasting regions with high ($> 99\%$) and low reflectance. In addition, we find the localized patterns don't change in an obvious manner when modify the filling factor F , instead, just a wholly shifting to the longer wavelength. The reflectance spectrum shown in Fig. 3(a) reveals that with a proper selection of the grating parameters (e.g. the thickness T , filling factor F and period Λ), an ultra-high ($> 99\%$) reflectivity over a spectral range can be achievable (as shown by the double arrow line). Fig. 3(b) shows the corresponding reflection spectrum calculated by setting $F = 0.50$, $\Lambda = 530$ nm, and $T = 230$ nm.

The optical characteristics of the structure composed of two HCGs sandwiched by a thin SiO₂ layer is investigated by varying the angle of incidence (θ , from -25° to 25°) with respect to the z -axis. As shown in Fig. 4(a), we observe symmetric patterns relative to the axis of $\theta = 0^\circ$ (also Γ point) and the disappearance of resonance features at discrete points of $\theta = 0^\circ$ (positions marked by '1', '2', and '3') and 14.8° (marked by '4'). Those vanishing linewidths suggest a non-leaky bound state within the continuous spectrum of radiating waves [4]. Fig. 4(b) presents the field distribution profiles in (x, z) -plane at discrete points (incident angle $\theta = 0^\circ$), which indicate the dark mode feature of BICs. For instance, the E_y distribution of mode 2 over the (x, z) -plane shows two radiators with equal amplitude but

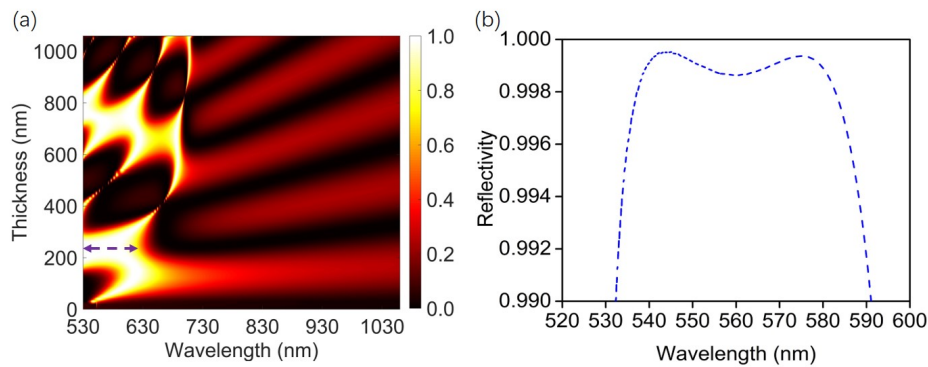


FIG. 3: (a) Reflectance spectra mapping as a function of grating thickness when the filling factor $F = 0.50$; (b) calculated reflectance spectrum of single grating layer by using $F = 0.50$, $\Lambda = 530$ nm, and $T = 230$ nm.

opposite phase at the top interface, canceling the upward out-of-plane radiation. Similarly, the two radiators at the bottom interface cancel the downward out-of-plane radiation. Hence, mode 2 is a symmetry-protected BIC, as the out of plane radiation vanishes due to the intrinsic symmetry [11]. By using the same analysis, we can recognize the mode 1 and mode 3 also as symmetry-protected BICs. The mode 4 located off the Γ point (also above the light line) is classified as Friedrich-Wintgen BIC [12], which is caused by the destructive interference of resonances at the correct phase-matching conditions [19].

To confirm the existence of BICs, we investigate the reflectance spectra properties of the structure with illumination at 0° and 14.8° (black curves in Fig. 4(c) and (d)), respectively. No modes are observed at the marked spectral positions, except the mode 2 around ~ 566 nm. Then, when the incident angle is tilted by 2° , distinct narrow peaks appear at the positions of mode 1, mode 3 and mode 4 (see red curves). Meanwhile, we find mode 2 shows an enhancement by using this oblique illumination. The large difference obtained by a small angle shifting indicates the unique feature of BIC — resonance singularity above light line, thus the BIC with infinite Q factor cannot be directly observed at the correct incidence wave vector. However, sharp spectral feature with narrow linewidth can distinctly appear near the BIC (shift the incidence by a small angle). Indeed, near the BIC, the resonance spectrum exhibits an asymmetric Fano line shape, but is collapses at the breaking point. Therefore, the distinct spectral features offer another confirmation for the BICs of mode 1, mode 3 and mode 4.

BICs have been found in various photonic structures [1, 4, 5, 13–16], and the mechanisms leading to BICs have been extensively discussed. Here, the formation of BICs at Γ point can refer to a destructive interference between two radiating channels with different optical behaviour — the FP modes and guided modes within this specific spectral domain, which contribute to the generation of dark modes. For the Friedrich-Wintgen BIC at off-

Γ point, we consider that it is mainly caused by the destructive interference between higher order FP mode and guided resonance mode. In principle, two HCG layers are considered as a pair of perfect mirrors, the transmission and resonant radiation in z -direction can destructively interfere when the spacing between HCG layers is satisfied a certain condition, making the round-trip phase shifts add up to an integer multiple of 2π [17]. Consequently, Fano resonance collapses to a Friedrich-Wintgen BIC state.

Closer investigation of mode 2 reveals that there is a broad frequency dispersion over the range of momentum around 566 nm, which indicates the quasi-BIC feature and strong resonance in individual unit cell [18]. Fig. 4(e) presents the evolution of quasi-BIC mode with incident angle, it is clear to find that the spectrum reaches a minimum intensity value at 0° , then the Fano resonance featured spectrum becomes broader and larger at off- Γ position. To evaluate the performance of observed the quasi-BIC at 566 nm, we calculated the quality factor of the resonance mode at λ position by using the formula $Q = \lambda/\Delta\lambda$, where $\Delta\lambda$ is the full width at half maximum (FWHM) of the spectrum. Fig. 4(f) shows the calculated Q -factor of the quasi-BIC mode obtained by sweeping the incidence angle. It is evident from the figure that the Q -factor of the mode reaches to 2×10^4 at Γ point, and this finite number further presents the property of quasi-BIC. The high- Q resonance enables the compact resonator to realize lasing over a large area in a single mode.

To further investigate the influences of structural parameters on the formation of BICs with normal incidence, we plot the reflectance spectra for the resonator with varied HCGs (T , Fig. 5(a)) and SiO_2 layer thicknesses (T_S , Fig. 5(b)), respectively. We find both of these two parameters play significant impact on the formation of BICs, and they only can be created when some certain conditions are satisfied. In detail, when we set the thickness of SiO_2 layer to be 215 nm and change HCGs' thicknesses (Fig. 5(a)), the corresponding BIC around 566 nm is observed when $T = 230$ nm, which appears on the boundary between two high-transmission

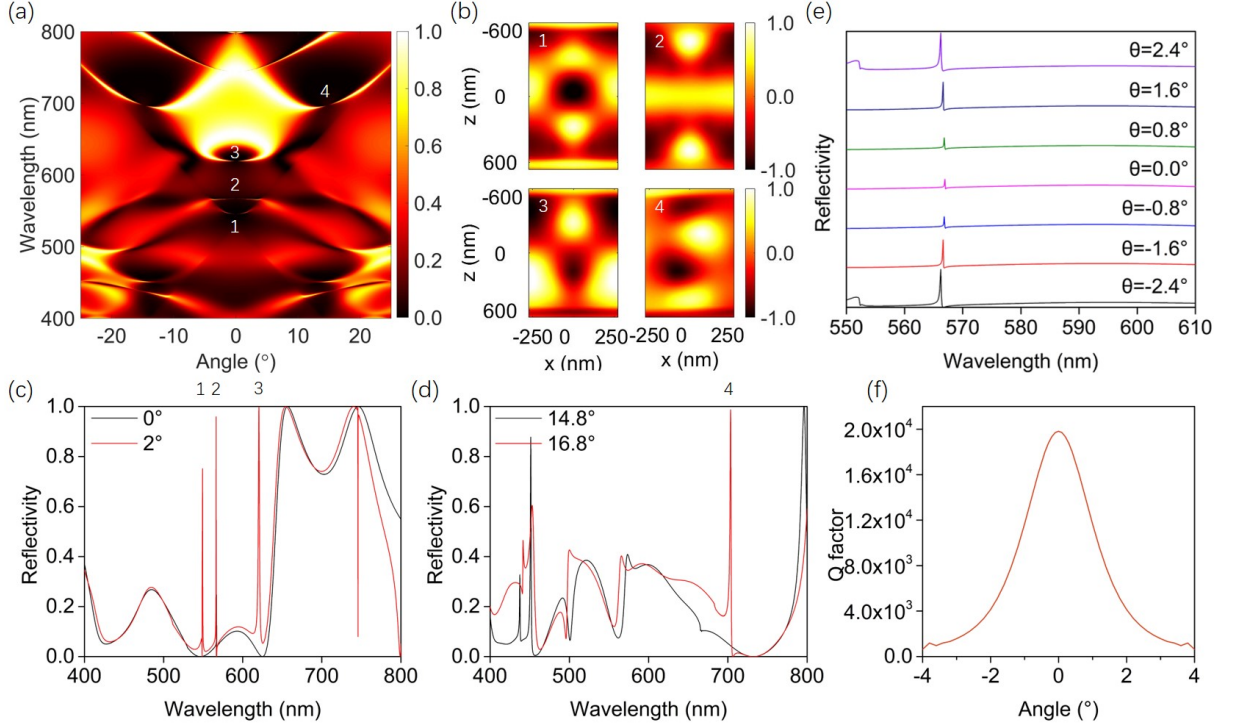


FIG. 4: (a) Resultant reflectance contour distribution of the architecture by sweeping the incident angle from -25° to 25° ; (b) electric field distribution profiles corresponding to the places marked by ‘1’, ‘2’, ‘3’ and ‘4’, respectively; (c) reflection spectra of resonator when the incident angle is 0° and 2° ; (d) reflection spectra of resonator when the incident angle is 14.8° and 16.8° ; (e) evolution of the quasi-BIC mode with incident angles; (f) angular dependence of Q -factor of the quasi-BIC mode.

channels. Additional BICs around 612 and 660 nm are also recognized when $T = 170$ and 410 nm, respectively. These BICs exhibit similar formation mechanism, but locate at different frequency positions. Then, when T is kept at 230 nm and T_S is variable (Fig. 5(b)), the discussed BIC around 566 nm is confirmed when $T_S = 215$ nm. It is worthy to note that such BIC presents periodical repetition (period thickness $T_P = 195$ nm) through increasing T_S , favoring the BIC engineering and device fabrication. Another BIC around 750 nm is observed when $T_S = 565$ nm. Therefore, we conclude that the refractive index symmetry environment supports the generation of SP-BIC, different BICs can appear by changing the thicknesses of HCGs; Changing the thickness of central SiO_2 layer leads to the modification of the phase shift between two radiation channels, thus favoring the periodical appearance of the supported BIC.

B. Quasi-BIC lasing and characterization

To realize quasi-BIC lasing, we selected the grating parameters ($T = 230$ nm, $F = 0.50$, and $\Lambda = 530$ nm) which can provide the highest possible reflectivity (as marked in Fig. 3), and the SiO_2 thickness is 215 nm. Then, R6G dye molecules are doped into SiO_2 thin layer to compensated the internal losses of resonator.

As shown in Fig. 1(b), the proposed sandwiched structure recalls conventional VCSELs, however our design significantly reduces the cavity length. Fig. 6(a) shows the gain spectrum of R6G (black curve), the spectrum of the cavity mode (blue curve) and typical lasing spectrum of resonator (red curve). Clearly, the R6G gain spectrum has a broad linewidth with its central region overlapping with the cavity mode peak, a feature guaranteeing a proper compensation of the cavity losses. Interestingly, the cavity mode shows the typical asymmetric line shape of a Fano resonance. This Fano resonance is caused by the interference of radiative (bright) and non-radiative (dark) modes [48, 49]. For Si_3N_4 -based HCG resonator, dark mode is associated with the Bragg scattering induced by HCG in the lateral direction, which results in a resonant mode with narrow bandwidth. On the other hand, the bright mode is associated with the weak Fabry-Perot mode induced by the index difference in the vertical direction, which results in a mode with nearly flat-band spectrum. The interference of these two modes result in an asymmetric line shape of the spectrum [44, 50]. Moreover, this phenomenon could confine the optical mode in the structure well and result in a high Q factor, which is beneficial for the BIC laser operation with very narrow linewidth (red curve).

Fig. 6(b) shows the detail characterizations of lasing

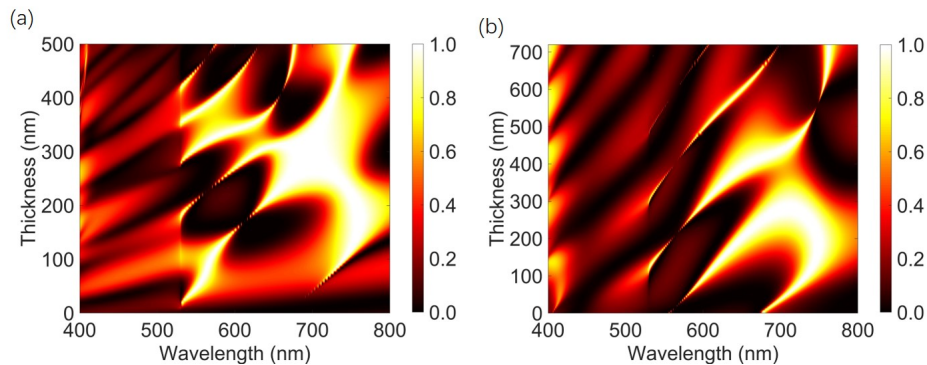


FIG. 5: Reflectance spectra as a function of the thickness of HCGs and SiO_2 , respectively: (a) with varied HCGs thickness; (b) with varied SiO_2 thickness.

behaviour. The black curve is the conventional plot of output power as a function of pump energy density, so we can estimate the threshold is around $17 \mu\text{J}/\text{cm}^2$. The blue curve represents the corresponding optical spectrum linewidth changing, the sharp narrowing of spectrum also indicates a coherence emission is achieved when the laser is operated above threshold. Both of two kinds of characterizations indicate the BIC laser has been successfully demonstrated.

Fig. 6(c) and (d) are the electric field intensity distributions of resonator in (x, y) and (x, z) planes, respectively. When the resonator is operated above threshold, a large mode overlaps with the input pump contributing to a simple and efficient coupling of the input light, as suggested by the high intensity interfere fringes. From the side view (Fig. 6(d)), it is clear how the light is predominantly confined within the grating bars and there is exactly one intensity lobe within the interval of neighboring bars. In the middle, higher intensity stripe indicates the gain medium region, where we can find the vertical confinement of this device is much stronger than the confinement typically found in conventional DBRs-based vertical cavity emitting lasers. Since the double gratings provide the largest power reflectance, all diffraction orders disappear except the 0th order. In addition, the HCGs bring a higher effective refraction index and much higher than the surrounding environment, leading to strong lateral confinement for the lateral modes.

IV. SENSING FUNCTION FOR GAS DETECTION

High- Q resonators with narrow resonance line widths and long photon storage time, have been considered as ideal candidates for sensors with enhanced detection sensitivity [51, 52]. Therefore, we carry out quantitative calculations of the quasi-BIC laser intrinsic sensitivity upon changes of the surrounding refractive index. We first reproduced a gas environment and immersed the resonator in a atmosphere of known refractive index

value, then performing a refractive index change from 1.0000 to 1.0020. Fig. 7(a) displays the full lasing spectra of the device *vs.* variation of refractive index, where it is easily observe a shift of the emission wavelength towards a longer wavelengths, even though the refractive index increase step was just of the order of 5×10^{-4} . The inset exhibits the laser spectra upon change of the gas environment, where we notice a single wavelength shifting without any other obvious changing. This also can be found from Fig. 7(b), which presents the linear dependence of emission peaks on the refractive index (black curve), and the linewidth variation (dash curve). It is further confirmed that the change of refractive index results in only the shift of lasing wavelength without affecting the lasing state. This simple linear relationship between lasing wavelength shift and the variation of environment confirms the sensing capability of the proposed microlaser structure.

Specifically, the sensing performance of the device was evaluated by estimating the sensitivity (S_λ) and figure of merit (FOM_λ), which can be calculated through using the following formulas:

$$S_\lambda = \frac{\Delta\lambda}{\Delta n}, \quad (4)$$

$$FOM_\lambda = \frac{S_\lambda}{\gamma} \quad (5)$$

where $\Delta\lambda$ represents the emission wavelength shifting, and Δn is the change of refractive index. γ is the emission spectrum linewidth measured at its full width at half maximum. FOM parameter is another important and more comprehensive benchmark to evaluate sensing performance [53, 54]. From the results in Fig. 7(b), we calculated the S_λ and FOM_λ , which are 221 nm/RIU and 4420 RIU $^{-1}$, respectively. Very importantly, the achieved FOM value resulted much higher than the theoretical result for localized surface plasmon resonance (LSPR) sensors (~ 20) [55], photonic crystal (PhC) cavity [31], microring [56] and fiber Bragg grating (FBG) sensors [57]. It is also comparable with that of state-of-the-art symmetry guided-mode resonance based

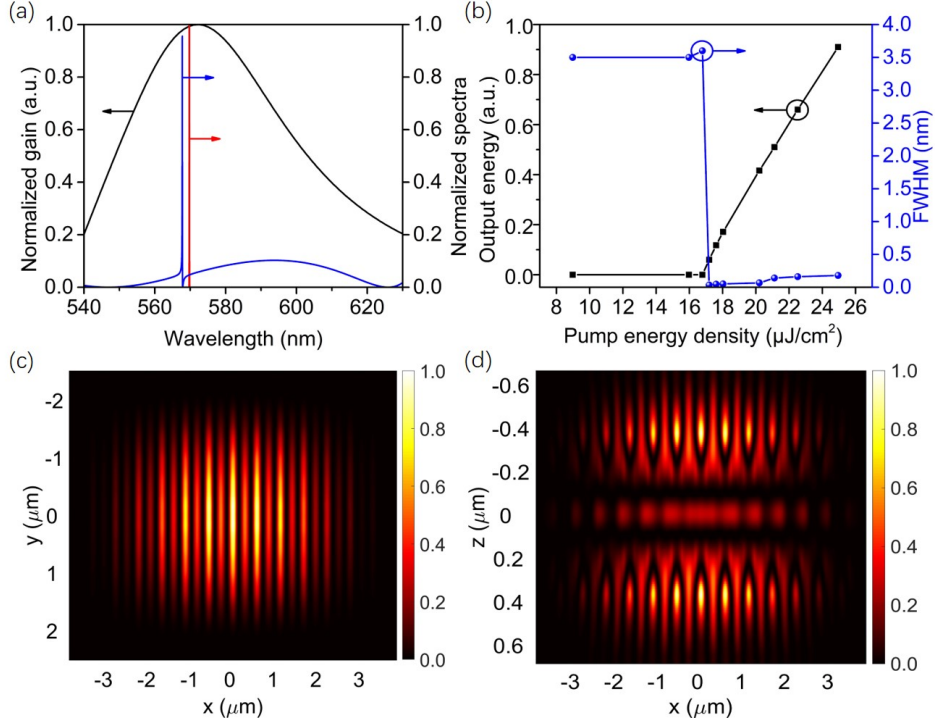


FIG. 6: (a) Gain spectrum of R6G (black curve), cavity mode spectrum (blue curve), and typical emission spectrum of laser (red curve) operated above threshold; (b) input-out function curve (black) and spectrum linewidth changing as a function of input energy (blue); (c) electric field intensity distribution of laser emission in (x, y) plane; (d) electric field intensity distribution in (x, z) plane.

sensors [53]. In addition, the organic gain enabled laser design leads to a coherent light source, which can either be detected at optical far field, or be easily coupled into fiber system. Thus, this flexible operation will facilitate the experimental measurements. In addition, the simple structure design will effectively reduce the cost of fabrication, making the sensor more appealing.

V. CONCLUSION

In conclusion, we have presented the design and numerical characterization of a compact quasi-BIC-laser based sensor for detecting of gas environment changing. The sensor is designed by using double Si_3N_4 HCG grating layers and organic R6G dye molecule doped SiO_2 layer located between the grating layers. The proposed unique hybrid design enables stimulated vertical emission from the organic gain medium embedded in the HCG stripes. Optimizations concerning HCGs and microcavity configuration designed for a 570 nm resonant wavelength have been performed. Our design features a high-Q resonance, which enables a narrow-linewidth laser emission of 0.05 nm. Therefore, a pronounced lasing behaviour with narrow spectrum linewidth have been realized. The emitted light is close to the plane wave in air, which indicates a single lobe far field pattern for laser beam distribution. The sensing mechanism

can be reasonably explained through the guided-mode resonance effect originated by constructive interference between the guided modes of the slab grating and the strong reflection modes. Finally, we also investigated the bulk sensing performance by inserting the device in some specific environment with different refractive index values, demonstrating remarkable sensitivity and figure of merit estimated equal to 221 nm/RIU and 4420 RIU^{-1} , respectively. Especially the figure of merit value outperforms recently reported GRM devices [53, 58] and other state-of-the-art passive sensors [31]. In view of these achievements, it is believed that this new platform could improve the current technology in remote gas sensing, e. g. warning from dangerous chemical gas.

Acknowledgment

We are grateful to Prof. Yang Li from Tsinghua University for useful discussions. T. Wang acknowledges financial support from the National Natural Science Foundation of China (Grant No. 61804036) and Zhejiang Province Commonweal Project (Grant No. LGJ20A040001). I. De Leon acknowledges the support of the Federico Baur Endowed Chair in Nanotechnology. L. Peng thank the support from the Natural Science Foundation of China (Grant No. 61875051) and Zhejiang Province Natural Science Foundation (LR21F010002).

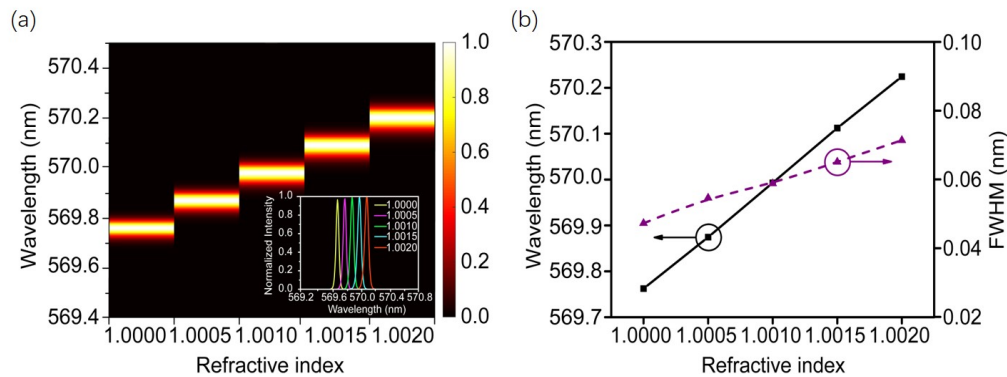


FIG. 7: (a) Mapping of emission wavelength shift with the variation of environment refractive index, inset: full lasing spectra for different refractive indexes; (b) linear relationship between emission wavelength shift and environment refractive index (black curve), and the corresponding spectrum linewidth changing with refractive index.

F. Gao thank the support from the Natural Science Foundation of China (Grant No. 61801426) and Zhejiang Provincial Natural Science Foundation (Grant No. Z20F010018). X. Lin thank the support from the Fundamental Research Funds for the Central Universities and Zhejiang University Global Partnership Fund.

Conflict of Interest

The authors declare no conflict of interest.

-
- [1] S. Joseph, S. Sarkar, S. Khan, and J. Joseph, “Exploring the optical bound state in the continuum in a dielectric grating coupled plasmonic hybrid system”, *Adv. Opt. Mater.*, DOI: 10.1002/adom.202001895. (2021).
- [2] J. von Neumann and E. Wigner, “On the behavior of eigenvalues in adiabatic processes,” *Phys. Z.*, **30**, 467 (1929).
- [3] S. Han, L. Cong, Y. K. Srivastava, B. Qiang, M. V. Rybin, A. Kumar, R. Jain, W. X. Lim, V. G. Achanta, S. S. Prabhu, Q. J. Wang, Y. S. Kivshar, R. Singh, “All dielectric active terahertz photonics driven by bound states in the continuum”, *Adv. Mater.*, **31**, 1901921 (2019).
- [4] C. Marinica, A. G. Borisov, and S. V. Shabanov, “Bound States in the continuum in photonics”, *Phys. Rev. Lett.*, **100**, 183902 (2008).
- [5] C. W. Hsu, B. Zhen, J. Lee, S. L. Chua, S. G. Johnson, J. D. Joannopoulos, and M. Soljačić, “Observation of trapped light within the radiation continuum”, *Nature*, **499**, 188-191 (2013).
- [6] T. Dong, J. Liang, S. Camayd-Munoz, Y. Liu, H. Tang, S. Kita, P. Chen, X. Wu, W. Chu, E. Mazur, and Y. Li, “Ultra-low-loss on-chip zero-index materials”, *Light: Science & Applications*, **10**, 10 (2021).
- [7] H. Tang, C. DeVault, S. A. Camayd-Munoz, Y. Liu, D. Jia, F. Du, O. Mello, D. I. Vulis, Y. Li, and E. Mazur, “Low-loss zero-index materials”, *Nano. Lett.*, **21**, 914-920 (2021).
- [8] A. A. Lyapina, D. N. Maksimov, A. S. Pilipchuk, and A. F. Sadreev, “Bound states in the continuum in open acoustic resonators,” *J. Fluid Mech.*, **780**, 370-387 (2015).
- [9] Y. X. Xiao, G. Ma, Z. Q. Zhang, and C. T. Chan, “Topological Subspace-Induced Bound State in the Continuum”, *Phys. Rev. Lett.*, **118**, 166803 (2017).
- [10] C. M. Linton and P. McIver, “Embedded trapped modes in water waves and acoustics”, *Wave Motion*, **45**, 16-29 (2007).
- [11] C. W. Hsu, B. Zhen, A. D. Stone, J. D. Joannopoulos, M. Soljagic, “Bound states in the continuum”, *Nat. Rev. Mater.*, **1**, 16048 (2016).
- [12] S. I. Azzam, V. M. Shalaev, A. Boltasseva, and A. V. Kildishev, “Formation of bound states in the continuum in hybrid plasmonic-photonics systems”, *Phys. Rev. Lett.*, **121**, 253901 (2018).
- [13] E. N. Bulgakov and A. F. Sadreev, “Bloch bound states in the radiation continuum in a periodic array of dielectric rods”, *Phys. Rev. A*, **90**, 053801 (2014).
- [14] I. V. Timofeev, D. N. Maksimov, and A. F. Sadreev, “Optical defect mode with tunable Q factor in a one-dimensional anisotropic photonic crystal”, *Phys. Rev. B*, **97**, 024308 (2018).
- [15] Y. Plotnik, O. Peleg, F. Dreisow, M. Heinrich, S. Nolte, A. Szameit, and M. Segev, “Experimental observation of optical bound states in the continuum”, *Phys. Rev. Lett.*, **107**, 183901 (2011).
- [16] M. I. Molina, A. E. Miroschnichenko, and Y. S. Kivshar, “Surface bound states in the continuum”, *Phys. Rev. Lett.*, **108**, 070401 (2012).
- [17] S. Fan and W. Suh, “Temporal coupled-mode theory for the Fano resonance in optical resonators”, *J. Opt. Soc. Am. A*, **20**, 569-572 (2003).
- [18] A. Taghizadeh and H. Chung, “Quasi bound states in the continuum with few unit cells of photonic crystal slab”, *Appl. Phys. Lett.*, **111**, 031114 (2017);
- [19] H. Friedrich and D. Wintgen, “Interfering resonances and

- bound states in the continuum,” *Phys. Rev. A*, **32**, 3231 (1985).
- [20] K. Koshelev, S. Kruk, E. Melik-Gaykazyan, J. H. Choi, A. Bogdanov, H. G. Park, and Y. Kivshar, “Subwavelength dielectric resonators for nonlinear nanophotonics”, *Science*, **367**, 288-292 (2020).
- [21] Z. F. Sadrieva, I. S. Sinev, K. L. Koshelev, A. Samusev, I. V. Iorsh, O. Takayama, R. Malureanu, A. A. Bogdanov, and A. V. Lavrinenko, “Transition from optical bound states in the continuum to leaky resonances: role of substrate and roughness”, *ACS Photonics*, **4**, 723-727 (2017).
- [22] A. Kodigala, T. Lepetit, Q. Gu, B. Bahari, Y. Fainman, and B. Kanté, “Lasing action from photonic bound states in continuum”, *Nature*, **541**, 196-199 (2017).
- [23] S. T. Ha, Y. H. Fu, N. K. Emani, Z. Pan, R. M. Bakker, R. Paniagua-Domínguez, and A. I. Kuznetsov, “Directional lasing in resonant semiconductor nanoantenna arrays”, *Nat. Nanotech.*, **13**, 1042-1047 (2018).
- [24] S. G. Lee, S. H. Kim and C. S. Kee, “Bound states in the continuum (BIC) accompanied by avoided crossings in leaky-mode photonic lattices”, *Nanophotonics*, **9**, 4373-4380 (2020).
- [25] D. N. Maksimov, V. S. Gerasimov, S. Romano, and S. P. Polyutov, “Refractive index sensing with optical bound states in the continuum”, *Opt. Express*, **28**, 38907-38916 (2020).
- [26] S. Romano, G. Zito, S. Torino, G. Calafiore, E. Penzo, G. Coppola, S. Cabrini, I. Rendina, and V. Mocella, “Label-free sensing of ultralow-weight molecules with all-dielectric metasurfaces supporting bound states in the continuum”, *Photonics Res.*, **6**(7), 726-733 (2018).
- [27] N. Bosio, H. Šípová-Jungová, N. O. Länk, T. J. Antosiewicz, R. Verre, and M. Käll, “Plasmonic versus all-dielectric nanoantennas for refractometric sensing: A direct comparison”, *ACS Photonics*, **6**, 1556-1564 (2019).
- [28] R. M. Ma, S. Ota, Y. Li, S. Yang and X. Zhang, “Explosives detection in a lasing plasmon nanocavity”, *Nature Nanotech.*, **9**, 600-604 (2014).
- [29] J. Sun, T. Wang, Z. Jafari, F. Gao, X. Lin, H. Chen, G. Wang, I. De Leon, “High-Q plasmonic crystal laser for ultra-sensitive biomolecule detection”, *IEEE J. Sel. Top. Quantum Electron.*, **27**, 1-7 (2021).
- [30] F. Yesilkoy, E. R. Arvelo, Y. Jahani, M. Liu, A. Tittl, V. Cevher, Y. Kivshar, and H. Altug, “Ultrasensitive hyperspectral imaging and biodetection enabled by dielectric metasurfaces”, *Nat. Photonics*, **13**(6), 390-396 (2019).
- [31] Y. Liu, S. Wang, D. Zhao, W. Zhou, and Y. Sun, “High quality factor photonic crystal filter at $k \approx 0$ and its application for refractive index sensing”, *Opt. Express*, **25**, 10536-10545 (2017).
- [32] C. Huang, C. Zhang, S. Xiao, Y. Wang, Y. Fan, Y. Liu, N. Zhang, G. Qu, H. Ji, J. Han, “Ultrafast control of vortex microlasers”, *Science*, **367**, 1018-1021 (2020).
- [33] M. Maleki, M. Mehran, and A. Mokhtari, “Design of a near-infrared plasmonic gas sensor based on graphene nanogratings”, *Journal of the Optical Society of America B*, **37**, 3478-3486 (2020).
- [34] A. Anedda, C.M. Carbonaro, F. Clemente, R. Corpino, S. Grandi, A. Magistris, and P.C. Mustarelli. “Rhodamine 6G-SiO₂ hybrids: A photoluminescence study”, *Journal of Non-Crystalline Solids*, **351**, 1850-1854 (2005).
- [35] H. Yanagi, T. Hishiki, T. Tobitani, A. Otomo, S. Mashiko, “Thin film lasing from a dye-doped silicartitania composite,” *Chemical Physics Letters*, **292**, 332-338 (1998).
- [36] J. Hong, A. M. Spring, F. Qiu and S. Yokoyama, “A high efficiency silicon nitride waveguide grating coupler with a multilayer bottom reflector,” *Sci. Rep.*, **9**, 12988 (2019).
- [37] Y. Liang, N. Ruan, S. Zhang, Z. Yu, and T. Xu, “Experimental investigation of extraordinary optical behaviors in a freestanding plasmonic cascade grating at visible frequency,” *Opt. Express*, **26**, 3271-3276 (2018).
- [38] X.L. Zhong and Z.Y. Li. “All-analytical semiclassical theory of spaser performance in a plasmonic nanocavity,” *Phys. Rev. B.*, **88**, 085101 (2013).
- [39] K. Wang, H. Qian, Z. Liu, and P. K. L. Yu, “Second-order nonlinear susceptibility enhancement in gallium nitride nanowires,” *Progress In Electromagnetics Research*, **168**, 25-30 (2020).
- [40] M. Dridi and G. C. Schatz, “Model for describing plasmon-enhanced lasers that combines rate equations with finite-difference time-domain”, *J. Opt. Soc. Am. B*, **30**, 2791-2797 (2013).
- [41] D. J. Trivedi, D. Wang, T. W. Odom, and G. C. Schatz, “Model for describing plasmonic nanolasers using Maxwell-Liouville equations with finite-difference time-domain calculations”, *Phys. Rev. A*, **96**, 053825 (2017).
- [42] W. Zhou, M. Dridi, J. Y. Suh, C. H. Kim, D. T. Co, M. R. Wasielewski, G. C. Schatz and T. W. Odom, “Lasing action in strongly coupled plasmonic nanocavity arrays”, *Nat. Nanotech.*, **8**, 1-6 (2013).
- [43] T. Grossmann, S. Schleede, M. Hauser, M. B. Christiansen, C. Vannahme, C. Eschenbaum, S. Klinkhammer, T. Beck, J. Fuchs, G. U. Nienhaus, U. Lemmer, A. Kristensen, T. Mappes, and H. Kalt. “Low-threshold conical microcavity dye lasers”, *Appl. Phys. Lett.*, **97**, 063304 (2010).
- [44] T. T. Wu, S. H. Wu, T. C. Lu, and S. C. Wang, “GaN-based high contrast grating surface-emitting lasers”, *Appl. Phys. Lett.*, **102**, 081111 (2013).
- [45] C. J. Chang-Hasnain and W. Yang, “High-contrast gratings for integrated optoelectronics”, *Advances in Optics and Photonics*, **37**, 379-440 (2012).
- [46] V. Karagodsky and C. J. Chang-Hasnain, “Physics of near-wavelength high contrast gratings”, *Opt. Express*, **20**, 10888-10895 (2012).
- [47] T. Sun, S. Kan, G. Marriott, and C. Chang-Hasnain, “High-contrast grating resonators for label-free detection of disease biomarkers”, *Sci. Rep.*, **6**, 27482 (2015).
- [48] M. F. Limonov, M. V. Rybin, A. N. Poddubny, and Y. S. Kivshar, “Fano resonances in photonics”, *Nat. Photon.*, **11**, 543-554 (2017).
- [49] H. Heo, S. Lee, and S. Kim, “Tailoring Fano resonance for flat-top broadband reflectors based on single guided-mode resonance”, *J. Lightwave Technol.*, **37**, 4244-4250 (2019).
- [50] Y. Zhou, M. C. Y. Huang, C. Chase, V. Karagodsky, M. Moewe, B. Pesala, F. G. Sedgwick, and C. J. Chang-Hasnain, “High-index-contrast grating (HCG) and its applications in optoelectronic devices”, *IEEE J. Sel. Top. Quantum Electron.*, **15**, 1485-1499 (2009).
- [51] D. K. Armani, T. J. Kippenberg, S. M. Spillane, and K. J. Vahala, “Ultra-high-q toroid microcavity on a chip”, *Nature*, **421**, 925-928 (2003).
- [52] J. Zhu, S. K. Ozdemir, Y. F. Xiao, L. Li, L. He, D.

- R. Chen, and L. Yang, "On-chip single nanoparticle detection and sizing by mode splitting in an ultrahigh-Q microresonator", *Nat. Photon.*, **4**, 46-49 (2010).
- [53] Y. Zhou, X. Li, S. Li, Z. Guo, P. Zeng, J. He, D. Wang, R. Zhang, M. Lu, S. Zhang, and X. Wu, "Symmetric guided-mode resonance sensors in aqueous media with ultrahigh figure of merit," *Opt. Express*, vol. 27, pp. 34788-34802, 2019.
- [54] Q. L. Huang, J. Peh, P. J. Hergenrother, and B. T. Cunningham, "Porous photonic crystal external cavity laser biosensor", *Appl. Phys. Lett.*, **109**, 071103 (2016).
- [55] J. M. Bingham, J. N. Anker, L. E. Kreno, and R. P. Van Duyne, "Gas sensing with high-resolution localized surface plasmon resonance spectroscopy", *J. Am. Chem. Soc.*, **132**, 17358-17359 (2010).
- [56] C. Chung-Yen, W. Fung, and L. J. Guo, "Polymer microring resonators for biochemical sensing applications", *IEEE J. Sel. Top. Quantum Electron.*, **12**, 134-142 (2006).
- [57] X. Li, S. Liang, Y. Zhang, Q. Yu, X. Sheng, S. Lou, X. Wang, W. Zhang, M. Dong, and L. Zhu, "Novel refractive index sensor based on fiber bragg grating in nano-bore optical fiber", *Opt. Quant. Electron.*, **51**, 117 (2019).
- [58] Y. H. Wan, N. A. Krueger, C. R. Ocier, P. Su, P. V. Braun, and B. T. Cunningham, "Resonant mode engineering of photonic crystal sensors clad with ultralow refractive index porous silicon dioxide", *Adv. Opt. Mater.*, **5**, 1700605 (2017).